Check for updates

LIMNOLOGY and OCEANOGRAPHY

ASLO

Limnol. Oceanogr. 69, 2024, 2775–2790
© 2024 The Author(s). *Limnology and Oceanography* published by Wiley Periodicals LLC on behalf of Association for the Sciences of Limnology and Oceanography.
doi: 10.1002/lno.12687

Biogeochemical cycling of trace elements and nutrients in ferruginous waters: Constraints from a deep oligotrophic ancient lake

David J. Janssen [1*] **Adrianus Damanik** [2,3] **Nicolas Tournier** [2,3] **Julie Tolu** [4] **Lenny Winkel** [4,5] **Sri Yudawati Cahyarini** [6] **Hendrik Vogel** [2,3]

[1]Department Surface Waters, Eawag—Swiss Federal Institute of Aquatic Science and Technology, Kastanienbaum, Switzerland
[2]Institute of Geological Sciences, University of Bern, Bern, Switzerland
[3]Oeschger Centre for Climate Change Research, University of Bern, Bern, Switzerland
[4]Department Water Resources and Drinking Water, Eawag—Swiss Federal Institute of Aquatic Science and Technology, Dübendorf, Switzerland
[5]Department of Environmental Systems Science, ETH Zürich, Zürich, Switzerland
[6]Research Center of Climate and Atmosphere, National Research and Innovation Agency (BRIN), Bandung, Indonesia

Abstract

Iron-rich, ferruginous waters were the dominant geochemical regime for most of Earth's history. Modern ferruginous waters are found in stratified, sulfur-poor lakes, and serve as crucial analogs for biogeochemical cycling throughout Earth's past. Here we present the first depth-resolved data of physical structure, nutrients and trace elements from Lake Poso (Indonesia), a deep oligotrophic ancient lake. Lake Poso is ferruginous, with anoxia below ~ 90 m depth, placing it among the world's largest ferruginous lakes. Physical stratification is weaker than other tropical anoxic lakes, indicating sensitivity for paleoclimate reconstructions. Trace elements and nutrients are predominantly shaped by the oxic–anoxic transition. Manganese– and Fe oxyhydroxide–driven biogeochemical cycling occurs at distinct depth horizons, with Co and Ni controlled by Mn and showing shallow release in anoxic waters, while V, Cr, P, and As are controlled by Fe, with release in surface sediments and diffusive transport. Chromium is nonquantitatively removed in anoxic waters, in contrast to widespread assumptions in Cr-based paleoreconstructions. Oxycline U and Se removal corresponds to a local N minimum, suggesting biological reduction and/or uptake. These first ferruginous water Se data also show removal in sediments, indicating sediment signals reflect multiple removal processes and informing Se-based paleoreconstructions, while the absence of sediment U removal contrasts other anoxic basins. A comparison with other ferruginous lakes demonstrates how local influences drive deviations from expectations in other systems, and highlight common, generalizable ferruginous basin features. Therefore, these data will guide research in ferruginous settings across space and time, and improve paleoreconstructions from ferruginous sediment records.

Interannual water column anoxia occurs in lake and marine systems when deep waters are prevented from O_2 renewal through limited vertical mixing and/or lateral transport. In modern settings, these anoxic waters play a major role in the global biogeochemical cycle of major nutrients (Van Cappellen and Ingall 1994; Carey et al. 2022), greenhouse gasses (Naqvi et al. 2010), and trace element micronutrients, toxins and tracers (Little et al. 2015). Large-scale monitoring indicates widespread O_2 loss in freshwater and marine environments over the last decades, and modeling studies predict expanding anoxia in the future (Schmidtko et al. 2017; Fukushima et al. 2017; Jane et al. 2023), underlying the importance of understanding biogeochemical cycling in anoxic systems.

Anoxic waters are typically categorized reflecting the dominant redox processes and accumulated reduced substances, that is, ferruginous (Fe rich) and euxinic (H_2S rich) (Canfield and Thamdrup 2009), serving as a concise characterization of

*Correspondence: david.janssen@eawag.ch

Additional Supporting Information may be found in the online version of this article.

This is an open access article under the terms of the Creative Commons Attribution License, which permits use, distribution and reproduction in any medium, provided the original work is properly cited.

Author Contribution Statement: HV and SYC designed the Lake Poso research project in general, and DJJ, AD and HV designed the water column component. AD, NT and HV conducted the fieldwork with support from SYC. DJJ prepared and analyzed the samples, with analytical assistance from JT. JT and LW advised on analysis and interpretations for As and Se. DJJ led interpretations and manuscript preparation, and all authors contributed to the manuscript.

broad-scale biogeochemical regimes. Ferruginous conditions are the dominant regime of aquatic systems throughout much of Earth's history (Planavsky et al. 2011; Poulton and Canfield 2011; Swanner et al. 2020). While high S availability in the modern ocean results in euxinic rather than ferruginous marine waters, as seen in coastal eutrophic sites and restricted basins (Meyer and Kump 2008), the limited S availability of lakes can favor ferruginous conditions when overturning occurs rarely (oligomictic) or is absent (meromictic) (Swanner et al. 2020). Therefore, ferruginous lakes provide analogs to constrain biogeochemical cycling under geochemical conditions similar to those of the early Earth (Swanner et al. 2020).

However, despite the importance of trace elements as paleoproxies (Tribovillard et al. 2006; Robbins et al. 2016; Bennett and Canfield 2020; Horner et al. 2021) and essential micronutrients (Robbins et al. 2016), as well as the importance of ferruginous conditions through Earth's history, only very few trace element data are available in ferruginous systems. These data are needed to (i) compliment model-based inferences of metal availability across geologic time, helping to resolve questions surrounding the roles of metal availability and the evolution of life (Robbins et al. 2016), and (ii) give much-needed mechanistic constraints to metal abundance and isotope records used in paleoreconstructions. A brief introduction of major controls of trace element in redox-stratified system and major remaining questions is presented here, and the reader is referred to the above-cited reviews for more detail.

The reduced forms of Cr and V, which are favored under anoxic conditions, are prone to adsorption (e.g., onto metal oxides), and therefore can be removed from anoxic waters, fueling sediment enrichments (e.g., Tribovillard et al. 2006). While quantitative Cr removal is assumed and is central to many Cr paleoredox applications (Wei et al. 2020), modern euxinic basin data indicate non-quantitative removal may be more likely (Janssen et al. 2022). Similar constraints are needed in ferruginous settings. Cobalt and Ni are similarly prone to oxide scavenging; however, they accumulate in anoxic deep water, and the mechanisms driving Ni enrichment in euxinic sediments are unclear, as dissolved Ni concentrations are not strongly depleted (e.g., Jacobs and Emerson 1982; Vance et al. 2016). Sulfur-poor ferruginous data may help to clarify mechanisms driving sediment records (i.e., the importance of sulfide or other controls), as well as the importance of Ni in anaerobic metabolism (e.g., methanogenesis, cf. Robbins et al. 2016). Copper and Cd are both highly sensitive to sulfide availability, therefore showing enrichments in reducing marine sediments (e.g., Tribovillard et al. 2006), though the degree to which these metals are removed from S-limited systems, and what process(es) drive removal, remain less clear. Similarly, Mo, U, and Re, all poorly soluble in euxinic waters, show variable sediment enrichments across gradients in water column redox in modern marine systems (e.g., Bennett and Canfield 2020). Expanding these constraints to ferruginous systems would improve potential uses of this multiproxy tracer. Finally, despite the emerging potential of Se as a paleoredox tracer (cf. Robbins et al. 2016), no ferruginous Se data are available, limiting process-based constraints for paleoreconstructions.

Here we present depth-resolved trace element and nutrient data in Lake Poso (Indonesia). Lake Poso is a large oligotrophic lake (Sulawesty et al., 2022; Damanik et al. 2023) with low-nutrient input from the catchment (~ 990 km^2) and minimal anthropogenic perturbation (Damanik et al. 2023). Our new data characterize biogeochemical cycling within the lake and contribute toward a much-needed set of trace element geochemical constraints from modern ferruginous settings, therefore improving understandings of biogeochemical cycling in these systems.

Background of the study site and previously studied ferruginous lakes

Lake Poso is an ancient tectonic lake in Central Sulawesi (Indonesia) located at 485 m above sea level. With a surface area of 364 km^2, a depth of around 400 m, and a volume of 75.3 km^3, Lake Poso is one of the largest and deepest lakes in Indonesia (Lehmusluoto et al. 1997; Vaillant et al. 2011; Damanik et al. 2023). Anoxic deep water with elevated Fe concentrations has been reported (Lehmusluoto et al. 1997), though without depth profiles. Lake Poso is a so-called ancient lake (see Hampton et al. 2018) with high rates of endemic biodiversity (von Rintelen et al. 2012) and has been the site of evolution-focused research (e.g., Vaillant et al. 2011; Albrecht et al. 2020); however, little biogeochemical research has been conducted. Lake Poso formed $\sim 10^6$ years ago, a similar age to the Malili Lakes (e.g., Lakes Matano & Towuti; Wilson and Moss 1999; Vaillant et al. 2011; Albrecht et al. 2020). Although Lake Poso is near this well-studied Malili Lake system, it lies within a different catchment and has much lower surface water trace element concentrations (cf. Crowe et al. 2008; Damanik et al. 2023). Therefore, the major biogeochemical and physicochemical differences between these adjacent ancient lakes provides a unique opportunity to study specific controls on biogeochemical cycling, climate, and species radiation through time.

Lake Poso is near the equator and seasonal temperature variation is minimal, with mean annual temperatures of ~ 25–26°C (*see* Supporting Information). The predominant weather regimes affecting the lake are a warm dry monsoon phase strongest in July to October, where evaporation results in cooler surface water temperatures, and a moist monsoon phase strongest from March to April (Aldrian and Dwi Susanto 2003; Hidayat 2019), where surface waters can warm resulting in a shallow seasonal thermocline. Rainfall is correlated with El Niño-Southern Oscillation, particularly from July to October, with extended dry conditions during El Niño promoting enhanced evaporative surface cooling (Aldrian and

19395590, 2024, 11, Downloaded from https://aslopubs.onlinelibrary.wiley.com/doi/10.1002/lno.12687 by Paul Scherrer Institut PSI, Wiley Online Library on [02/12/2024]. See the Terms and Conditions (https://onlinelibrary.wiley.com/terms-and-conditions) on Wiley Online Library for rules of use; OA articles are governed by the applicable Creative Commons License

Dwi Susanto 2003; Hidayat 2019) (Supporting Information Fig. S1).

Previous ferruginous lake trace element studies have been conducted at Lake Pavin (France), Lake Matano (Indonesia), and Lake Hall (USA). One major challenge of paleoreconstructions and using ferruginous systems as early Earth analogs is differentiating biogeochemical features that can be extrapolated across space and time from local, site-specific features. Furthermore, despite the utility of the geochemical classifications ferruginous and euxinic, redox potential is a continuum, with specific metabolic and abiotic reactions occurring at different points along this continuum (Davison 1993; Rue et al. 1997). Therefore, waters within a broad regime may still vary in their specific biogeochemical processes and chemical signals. By compiling data from different environments, better constraints can be derived on both local controls and widespread redox processes, isolating generalizable signals left in the sediment archive that reliably reflect redox regimes.

With this in mind, a brief overview of local controls on trace elements in Lakes Pavin, Matano and Hall is presented. Lake Pavin (France), a volcanic lake with ion-rich, subaquatic input, shows strong enrichments of major ions (Michard et al. 1994) and many trace elements (Viollier et al. 1995) at depth, indicating both local controls (i.e., metal-rich subaquatic input) and internal biogeochemical cycles drive observed distributions (Michard et al. 1994; Busigny et al. 2016). In Lake Matano (Indonesia), a large, deep and ancient lake within a metal-rich ultramafic catchment with mining activity (Lehmusluoto et al. 1997), surface water concentrations of many trace metals are 10^1–10^2 times higher than typical for oxic fresh and marine waters (cf. Crowe et al. 2008; Gaillardet et al. 2014; Geotraces 2021), indicating trace element profiles may reflect strong local influence. Finally, Lake Hall (USA) is a small, shallow eutrophic system with clear anthropogenic influence (Balistrieri et al. 1994). Hundreds of other ferruginous lakes are known, many with reported Fe and some major element data (Swanner et al. 2020), and a couple has additional data for a few trace metals (e.g., the small and shallow Canyon and Brownie lakes; Lambrecht et al., 2018; Cole et al., 2020), though the vast majority of ferruginous lakes have not been studied.

Methods

Sampling

A depth profile was collected in the center of the lake (1°53′S, 120°35′E; Fig. 1a) on November 8–9, 2022 during the wet season and sunny weather conditions. Oxygen and temperature data were determined with a Sea and Sun CTD48M. Water density was calculated from in situ temperature, conductivity, and major ion composition, following Wüest et al. (1996). Water samples were collected from a 5-liter Niskin bottle (HydroBios), with the CTD below the Niskin bottle for precise depth determination. Dissolved samples were gravity filtered through acid cleaned Acropak capsule filters (0.2 μm PES) into acid-cleaned LDPE bottles, and unfiltered samples (for Fe, Mn, P, and N) were filled directly into acid-cleaned LDPE bottles (both collected in duplicate). Trace element samples were acidified to a final concentration of $\sim$ 0.024 M HCl (final pH $\sim$ 1.7) with sub-boiling distilled concentrated HCl (prepared using a Teflon still [Savillex]). Particulate Fe and Mn concentrations were determined by difference between filtered and unfiltered, and therefore reflect labile authigenic phases (e.g., amorphous oxides), but possibly not more inert phases (e.g., silicate minerals).

A chain of temperature loggers (Aqualogger 520 PT) was deployed in November 2022 and recovered in February 2024. An additional CTD profile with a Sea and Sun 60M CTD was conducted following logger recovery (February 29, 2024) (Supporting Information Fig. S1).

Analyses

Major anions and cations were determined by ion chromatography with Metrohm Compact IC instruments. Sulfate samples were not preserved (e.g., with Zn acetate), and therefore may reflect some reoxidation of H_2S. However, given the persistence of some H_2S-insoluble metals (e.g., Mo; *see* below) and H_2S data from nearby lakes (Crowe et al. 2008), it is unlikely that such oxidation is a major contributor to our determined SO_4^{2-} values. Field duplicate trace element subsamples were weighed out and dried in Teflon vials in laminar flow hoods, refluxed overnight with 0.25 mL concentrated subboiling distilled HNO_3 to oxidize organic matter, redried, and dissolved in 0.2 M HNO_3 for analysis. Trace element (Al, P, Ti, V, Cr, Mn, Fe, Co, Ni, Cu, As, Se, Mo, Cd, Ba, Re, and U) concentrations were determined with an Agilent 8900 ICP-MS/MS as detailed in the Supporting Information, with each subsample analyzed in duplicate ($n = 4$ analyses per depth). Accuracy was monitored with the SLRS-6 reference material (National Research Council of Canada) with determined values showing good agreement with certified and literature data (Yeghicheyan et al. 2019) (Supporting Information Table S2). Total N (TN), total dissolved N (TDN), total P (TP), and total dissolved P (TDP) were determined on acidified samples by standard spectrophotometric methods. In oxic waters, where P concentrations were very low, TP and TDP were determined by ICP-MS/MS (*see* Supporting Information Table S2 for detection limits).

Results and discussion

The general physicogeochemical structure of Lake Poso

Lake Poso is redox-stratified, with O_2 concentrations decreasing to zero near 90 m depth, slightly below the maximum observed mixing depth (Supporting Information Fig. S1), and remains anoxic below this depth (Fig. 1b; Supporting Information Fig. S1). Differences in temperature ($\sim$ 2°C), conductivity ($\sim$ 17 μS cm^{-1}) (Fig. 1c) and major ion concentrations (< 10%) are minor between surface and deep waters in 2022 and 2024

19395590, 2024, 11, Downloaded from https://aslopubs.onlinelibrary.wiley.com/doi/10.1002/lno.12687 by Paul Scherrer Institut PSI, Wiley Online Library on [02/12/2024]. See the Terms and Conditions (https://onlinelibrary.wiley.com/terms-and-conditions) on Wiley Online Library for rules of use; OA articles are governed by the applicable Creative Commons License

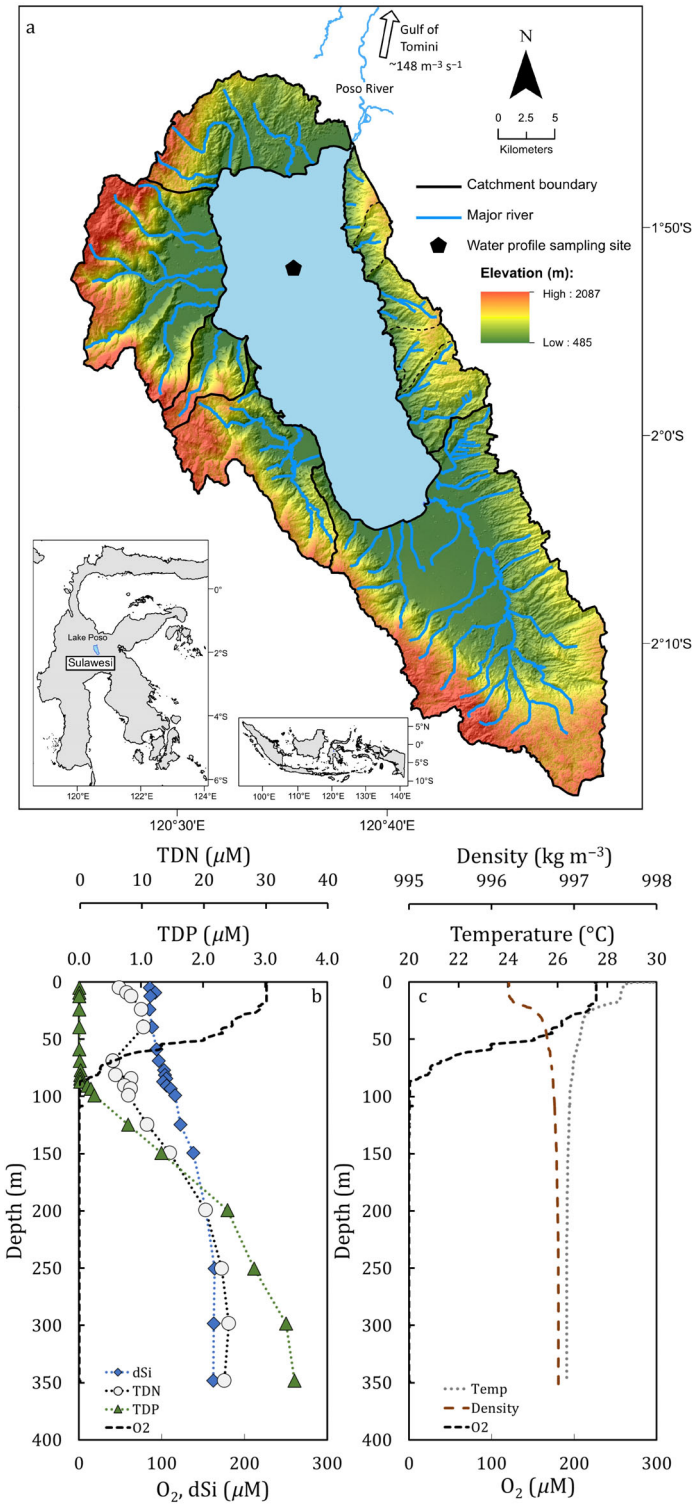

Fig. 1. Location and major physicogeochemical setting of Lake Poso. (**a**) Map of Lake Poso along with the sampling location (adapted from Damanik et al. 2023). (**b**) Major nutrient (TDP, TDN, and dSi) profiles. (**c**) Temperature, density, and O_2 profiles. dSi, dissolved silicate; TDN, total dissolved nitrogen; TDP, total dissolved phosphorus.

(Supporting Information Tables S4–S6; Fig. S1). Lake Poso's stratification, nearly entirely temperature driven, is stable on as annual basis (Supporting Information Fig. S1), and surface-to-deep temperature gradients are similar to those commonly seen in meromictic tropical lakes (e.g., Katsev et al. 2017). Stratification is roughly 2–4× weaker than other anoxic lakes—the nearby Lake Matano (Katsev et al. 2010) and Lakes Tanganyika and Malawi (Katsev et al. 2017)—and is much > 10× weaker than in Lakes Pavin and Kivu (Aeschbach-Hertig et al., 2002; Katsev et al. 2017) (Supporting Information Section S.3). This indicates that Lake Poso may be more prone to irregular overturning (i.e., oligomictic) with exceptional cooling, for example, by extreme events or changes in climate. With a volume of 75.3 km^3, annual surface discharge of ~ 4.7 km^3 (Damanik et al. 2023) and assuming ~ 1.3 m yr^{-1} evaporative loss (as reported in the nearby and similarly large Lake Towuti, Vogel et al. 2015), a 1st-order estimate of the hydraulic residence time of Lake Poso is ~ 15 yr. Given poor exchange between surface and deep waters, this is likely shorter in the surface and longer in the deep, and can be refined by more precise discharge, evaporation, and exchange data.

Surface nutrient concentrations are low (≤ 0.01 μM TDP, ≤ 13 μM TDN), with P likely the main limiting nutrient, based on N : P ratios (TDN : TDP > 100). This is consistent with prior reports of only low surface phytoplankton abundance in Lake Poso (Sulawesty et al., 2022). High Secchi depths (avg = 25.3 m, Kaban et al. 2023) suggest the euphotic zone may reach ~ 90 m (*see* Lee et al. 2018), within the nutricline (~ 70–100 m depth; Fig. 1b), and matching deep photosynthetic zones observed in other oligotrophic lakes (e.g., Coon et al. 1987; Sabo et al. 2009). Indeed, a minimum in TDN from ~ 70 to 90 m (Fig. 1b) suggests some biological N uptake or removal in this zone.

Depth profiles of nutrients and trace elements are largely governed by responses to the transition between the oxic epilimnion and anoxic hypolimnion (Figs. 1–3; Supporting Information Fig. S3). Here, TDP increases by two orders of magnitude and TDN and dissolved Si (dSi) concentrations roughly double (Fig. 1b). Dissolved Mn (dMn) and dFe concentrations increase from the oxic–anoxic interface (85–90 m depth) (Figs. 2, 3a), with the maximum dMn (~ 5.5 μM) reached by 200 m depth, while dFe continues increasing smoothly until the deepest sample (350 m depth, ~ 35 μM), within the dFe range proposed for Precambrian Earth's ferruginous oceans (Swanner et al. 2020). Minor SO_4^{2-} decreases with depth (~ 25%, or ~ 6 μM), with a minimum in the deepest samples, reflect some reduction in deep waters and/or sediments (Fig. 2; Supporting Information Fig. S3a). Sulfur availability is insufficient to trap the Fe(II) that accumulates in the anoxic zone through sulfide formation, a characteristic of ferruginous systems (e.g., Canfield and Thamdrup 2009; Swanner et al. 2020), and Lake Poso is one of the world's largest ferruginous lakes (*see* Swanner

19395590, 2024, 11, Downloaded from https://aslopubs.onlinelibrary.wiley.com/doi/10.1002/lno.12687 by Paul Scherrer Institut PSI, Wiley Online Library on [02/12/2024]. See the Terms and Conditions (https://onlinelibrary.wiley.com/terms-and-conditions) on Wiley Online Library for rules of use; OA articles are governed by the applicable Creative Commons License

et al. 2020). The dFe_{max} observed in Lake Poso is lower than in many other ferruginous lakes (Supporting Information Table S3), and the rate of dFe increase below the chemocline is more gradual than in previously studied deep ferruginous Lakes Pavin (Michard et al. 1994), Matano (Crowe et al. 2008), and Nyos (Teutsch et al. 2009; Supporting Information Fig. S2). This likely reflects local differences in Fe budgets, and particularly deep Fe inputs in Lakes Pavin and Nyos (Teutsch et al. 2009; Busigny et al. 2016) which act to increase dFe gradients in these lakes. Ferricline slopes normalized to dFe_{max} are similar in Lakes Poso and Matano, reflecting that while catchment lithology contributes elevated Fe input into Lake Matano (e.g., ultramafic, Fe-rich weathering products, Crowe et al. 2008; cf. Damanik et al. 2023), similar internal physicobiogeochemical cycling results in similar ferricline dynamics (Supporting Information Fig. S2).

FeMn oxide regulation on trace element distributions

As expected in redox-stratified basins (e.g., Davison 1993), a zone of elevated particulate Fe and Mn (pFe, pMn) phases forms shortly above the oxic–anoxic interface (Fig. 3d). In Lake Poso, the pFe peak is more abrupt, larger in magnitude, and sits slightly deeper (at 91 m) than the more diffuse pMn maximum (at ~ 78–88 m), which disappears by 91 m. This slight offset is caused by differences in redox potentials and oxidation kinetics of Mn and Fe (Davison 1993), as well as the reductive dissolution of sinking Mn oxides (MnOx) driving the oxidation of Fe(II) and forming Fe oxyhydroxides (FeOx) (e.g., Dellwig et al. 2010). However, FeOx and MnOx maxima can often appear very close together in natural systems, such that their depth ranges may not be differentiated (e.g., Jones et al. 2011). As regularly observed in redox-stratified waters, the concentrated zone of FeOx and MnOx acts as a major control on the distributions of elements prone to scavenging onto metal oxides (e.g., Balistrieri et al. 1994; Taillefert et al. 2002; Crowe et al. 2008; Dellwig et al. 2010). This is seen in broadly coincident local minima in dissolved Ni, V, and Cr (dNi, dV, dCr) profiles near 85–90 m depth, as well as in dissolved Co (dCo), As (dAs), and TDP profiles, which increase at the base of this oxide zone (Fig. 3).

While FeOx and MnOx can be efficient scavengers, they show different specificities among trace elements (e.g., Koschinsky and Hein 2003), as seen in the detailed structure and concentration gradients in Lake Poso. Dissolved Ni shows an absolute minimum coincident with the pMn zone, and concentrations increase with dMn despite a maximum in pFe (Fig. 3b,e). Dissolved Co concentrations also increase immediately below the pMn zone, coincident with increases in dMn (Fig. 3c,f). This reflects efficient scavenging of Ni and Co onto MnOx, with release back to deep waters as MnOx are reductively dissolved below the oxic–anoxic interface (e.g., Lienemann et al. 1997; Taillefert et al. 2002). In contrast, dV and dCr minima occur at the same depth as the pFe maximum, and dissolved concentrations increase only below this pFe maximum (Fig. 3b,e). Similarly, dAs and TDP concentrations resemble dFe and increase more gradually, driven by upward diffusion of their dissolved phases following release from particles in deeper waters and/or sediments. Dissolved As and TDP are efficiently retained in anoxic waters due to retrapping onto metal oxides near the redox interface (e.g., Dellwig et al. 2010), preventing further upward diffusive transport and resulting in stable low dAs and TDP concentrations in surface waters (Fig. 3c,f). Although Mo can adsorb onto metal oxides (e.g., Goldberg et al. 2009), no significant change in dMo is seen across the metal oxide zone (Supporting Information Fig. S3b,e). This suggests that such oxides are not major drivers of water column dMo in general or that much higher metal oxide levels are needed for significant Mo removal within residence times and diffusive transport in Lake Poso.

The contrasts between Mn-like and Fe-like elements are easily seen in concentration depth profile 1st derivatives (Supporting Information Fig. S4). $\partial/\partial z$ profiles of dNi, dCo, and dMn show positive values at and slightly below the oxic–anoxic interface, and reach near zero by ~ 200 m. This suggests elements scavenged onto MnOx are added back to the water column shortly below the interface, with diffusive transport smoothing out concentration gradients. Similar observations, with Mn oxides reduced in the water column rather than sediments, have been made in other anoxic basins (e.g., Viollier et al. 1997; Dellwig et al. 2010; Jones et al. 2011). Negative $\partial/\partial z$ within the anoxic zone for dNi and to a lesser extent dCo (Fig. 3b,c; Supporting Information Fig. S4f), indicate removal in deeper waters or sediments, possibly as metal sulfides as reported in the nearby ferruginous lakes Matano and Towuti (Crowe et al. 2008; Vuillemin et al. 2023) (see below). Concentration maxima, $\partial/\partial z$ minima, and extents of linear dNi–dMn and dCo–dMn relationships occur at different depths for dCo and dNi (Fig. 3b,c; Supporting Information Figs. S4f, S5d), indicating divergent behavior of these elements, reflecting differing sensitivities of Ni and Co to sulfide formation or other burial phases. This may include kinetic inhibition of Co sulfide formation, with Co more likely incorporated into Fe sulfides (e.g., Swanner et al. 2014 and references therein).

In contrast to Mn-driven metals, $\partial/\partial z$ for dFe, dCr, and TDP (dV and dAs not shown but equivalent) show subdued maxima and remain positive throughout the anoxic zone (Supporting Information Fig. S4g), indicating deep-water distributions are controlled by release from particles near the sediment–water interface along with diffusive transport, unlike Mn. This is supported by strong linear correlations between dFe and major ions (e.g., Ca), as well between dFe and TDP, dV and dCr, below the oxic–anoxic interface (Supporting Information Fig. S5a,c). Prior reports from deep ferruginous lakes have observed the same, with particulate Fe phases reaching the sediments and transformations at the sediment surface driving benthic fluxes of P as well as Fe and

19395590, 2024, 11, Downloaded from https://aslopubs.onlinelibrary.wiley.com/doi/10.1002/lno.12687 by Paul Scherrer Institut PSI, Wiley Online Library on [02/12/2024]. See the Terms and Conditions (https://onlinelibrary.wiley.com/terms-and-conditions) on Wiley Online Library for rules of use; OA articles are governed by the applicable Creative Commons License

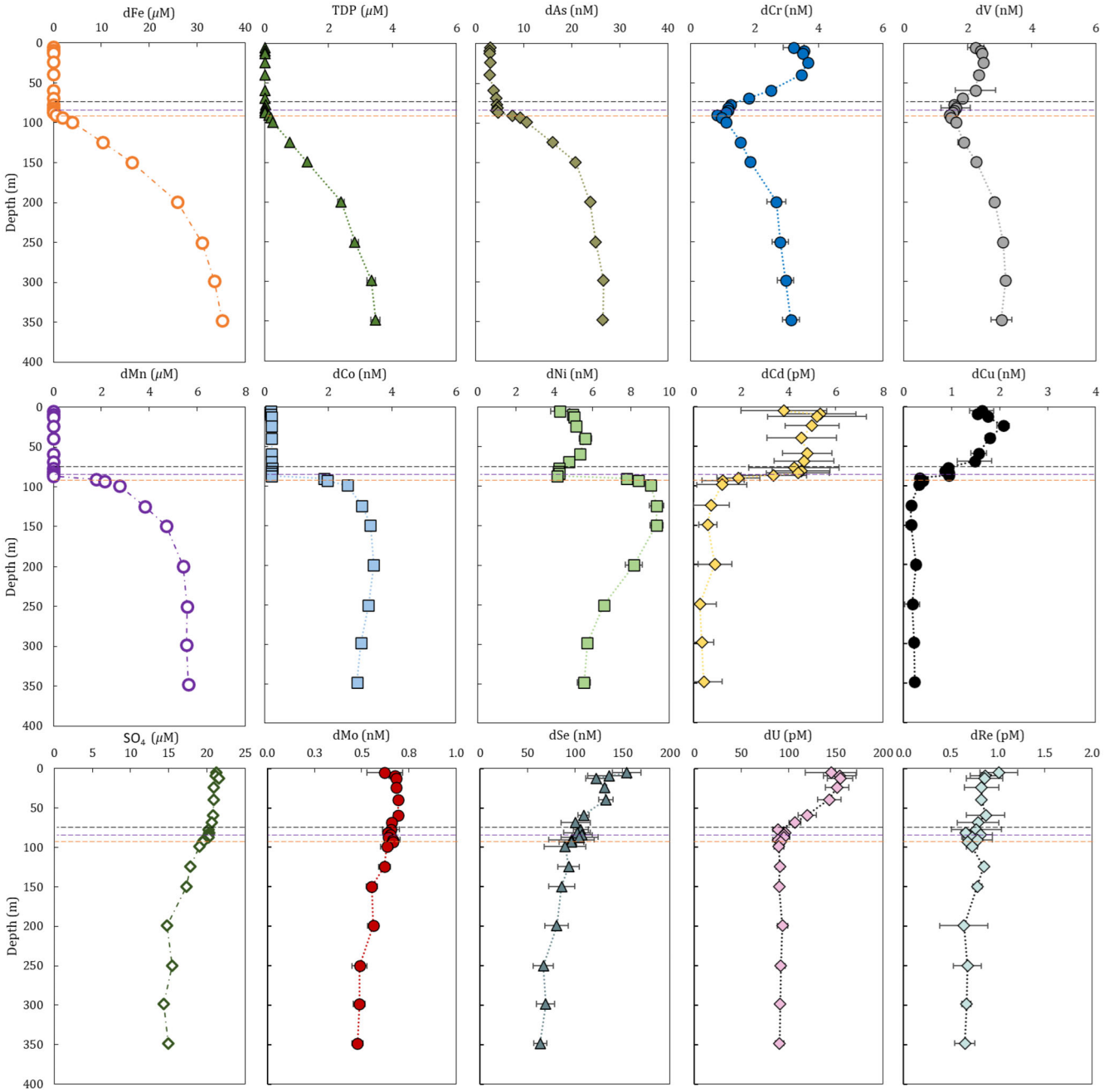

Fig. 2. Individual depth profiles of dissolved trace elements and SO_4^{2-}. Note the different *x*-axis scalings. Error bars show analytical uncertainty based on replicates, when larger than symbol size. Dashed black, purple, and orange lines indicate the TDN minimum and the zones of MnOx and FeOx formation, respectively. TDN, total dissolved nitrogen.

other elements (Viollier et al. 1995, 1997; Katsev et al. 2010; Busigny et al. 2016).

Sulfide and redox regulation on trace elements

Redox processes also influence trace element distributions through transformations into scavenging-prone or particulate species (e.g., Se^0, U(IV)), as well as their precipitation as particulate sulfides following the reduction of SO_4^{2-} to H_2S. Sulfate concentrations in Lake Poso decrease with depth (Supporting Information Fig. S3), with SO_4^{2-} minima in the deepest samples (~25% less SO_4^{2-} in deepest samples than the surface, or ~6 μM). A strong negative correlation between SO_4^{2-} and Ca (Supporting Information Fig. S5a) is consistent with water column diffusive control, suggesting SO_4^{2-} reduction may occur primarily within the sediments, and SO_4^{2-} concentration gradients extending well into the oxic layer reflect downward

19395590, 2024, 11, Downloaded from https://aslopubs.onlinelibrary.wiley.com/doi/10.1002/lno.12687 by Paul Scherrer Institut PSI, Wiley Online Library on [02/12/2024]. See the Terms and Conditions (https://onlinelibrary.wiley.com/terms-and-conditions) on Wiley Online Library for rules of use; OA articles are governed by the applicable Creative Commons License

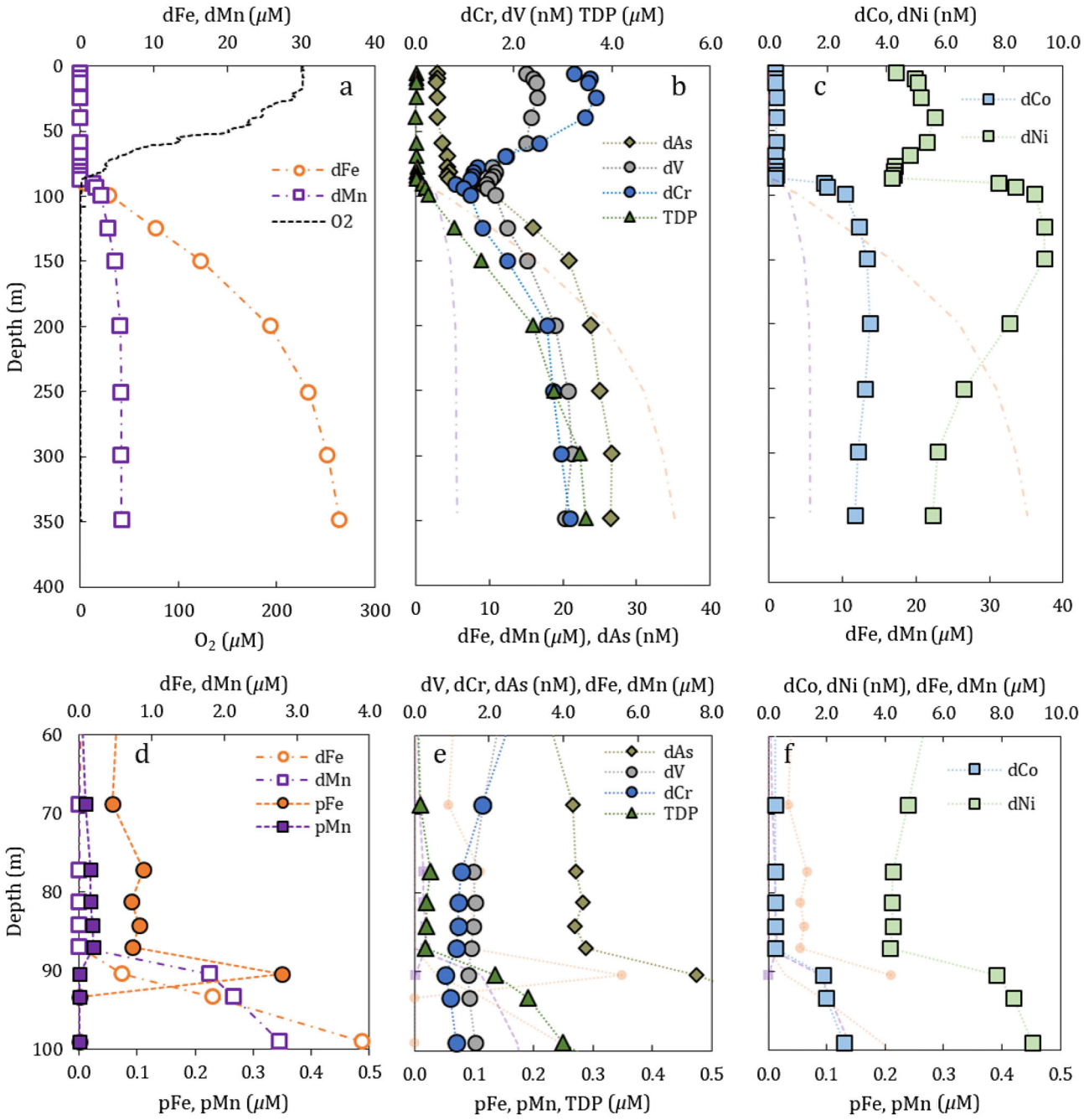

Fig. 3. Depth profiles of O_2, Fe, and Mn, and scavenging-prone trace elements (dV, dCr, dNi, dCo, dAs) and TDP. The full water column (top) and the oxic-anoxic interface (bottom) are shown. Panels a & d: pFe and pMn as filled symbols, dFe and dMn as open symbols. Traces of these profiles are presented in the other panels for orientation. dAs, dissolved As; dCo, dissolved Co; dCr, dissolved Cr; dFe, dissolved Fe; dMn, dissolved Mn; dNi, dissolved Ni; dV, dissolved V; TDN, total dissolved nitrogen.

diffusive fluxes from the oxic zone. Given the high dFe, low SO_4^{2-} and the role of Fe(II)-rich waters in buffering H_2S accumulation (e.g., Swanner et al. 2020), only low H_2S concentrations are expected in Lake Poso. Nevertheless, SO_4^{2-} reduction in Lake Poso indicates sulfide-insoluble (i.e., chalcophile) metals can be removed from the water column (e.g., Jacobs and Emerson 1982). Based on ambient metal concentrations, trace (< 1 nM) H_2S levels are sufficient for the formation of particulate metal sulfides from the most insoluble chalcophiles (Supporting Information Fig. S6).

Decreases in dissolved Cu (dCu) and Cd (dCd) are seen coincident with the MnOx and FeOx zones, before further decreasing in the anoxic zone (Supporting Information Fig. S3c,f). ∂/∂z dCu and dCd profiles reflect this well, with

19395590, 2024, 11, Downloaded from https://aslopubs.onlinelibrary.wiley.com/doi/10.1002/lno.12687 by Paul Scherrer Institut PSI, Wiley Online Library on [02/12/2024]. See the Terms and Conditions (https://onlinelibrary.wiley.com/terms-and-conditions) on Wiley Online Library for rules of use; OA articles are governed by the applicable Creative Commons License

sharp negative peaks in the metal oxide zone (~ 80–90 m), followed by recovery toward $\partial/\partial z = 0$ by 100 m, and then more gradual negative excursions from 100 to 150 m (Supporting Information Fig. S4d,h). Therefore, removal may occur as two steps, with a 1st and sharper metal decrease corresponding with metal oxides (i.e., adsorption), and a 2nd step (i.e., as metal sulfides) in the underlying anoxic zone (Supporting Information Fig. S3c,f). Unlike the elements following FeOx and MnOx-driven distributions, neither dCu nor dCd increase in the anoxic zone. Therefore, if metal oxide carrier phases are active in transport to anoxic deep waters, Cu and Cd are not resolubilized following FeMnOx reduction and the ultimate burial, likely as sulfides, is efficient despite minimal SO_4^{2-} reduction.

Abundances of Mo, Re, and U in sediments are widely used proxies for anoxic environments, and therefore these elements are expected to be removed from anoxic waters (e.g., Colodner et al. 1995; Tribovillard et al. 2006). Molybdenum is sulfide insoluble through the formation of particle-reactive thiomolybdates, though conversion is only complete at $H_2S \approx 11\ \mu M$ (Helz et al. 2011). Dissolved Mo correlates well with SO_4^{2-} throughout the whole water column (Supporting Information Fig. S5b) and the magnitude of the anoxic zone deficit relative to the oxic zone (< 30%) is similar to that of SO_4^{2-}. Given the smooth Mo decrease toward the deepest samples (cf. Supporting Information Figs. S3b, S5b) and correlations with conservative elements (Supporting Information Fig. S5a), the majority of Mo removal in Lake Poso likely occurs in the sediments, with diffusive transport controlling depth profiles, consistent with low expected water column H_2S levels. This contrasts existing dMo data from ferruginous (e.g., Lake Pavin, Viollier et al. 1995) and mildly euxinic (e.g., Lake Cadagno: Dahl et al., 2010) lakes, where a higher degree of SO_4^{2-} reduction occurs in the upper anoxic zone, coincident with a sharp Mo removal signal. Dissolved Re concentrations are very low (~ 1 pM) and show a slight decrease in anoxic waters relative to oxic surface waters (Fig. 2), though this is much smaller than seen in euxinic waters. In contrast to euxinic basins, dRe distributions are not controlled by ReS_2 solubility (Xiong 2003). Based on small dRe gradients with depth, it is not clear if removal is primarily across the oxic–anoxic interface, in sediments, or both. Finally, dU distributions in Lake Poso show a strong decrease near the oxic–anoxic interface, with concentrations in oxic surface waters approximately twice those in anoxic waters, and with little variability outside of the oxycline (Supporting Information Fig. S3b,e). The dU decrease is concurrent with a local TDN minimum, suggesting a potential role of biological reduction altering dU solubility (*see* below), which is supported by the stable dU minimum before accumulation of inorganic U reductants such as Fe(II). Dissolved U concentrations do not show specific minima corresponding to oxide maxima, despite their potential to scavenge U (Waite et al. 1994; Brennecka et al. 2011), nor increase following water column or sediment reduction of oxides (Fig. 2; Supporting Information Fig. S3). Dissolved Mo, dRe, and dU trends in Lake Poso differ from euxinic basins, where both dMo and dRe are removed within the euxinic water column, while dU removal is primarily in euxinic sediments (e.g., Colodner et al. 1995). This contrast is partly due to different sulfide levels, which control dMo and dRe solubility in euxinic settings (Xiong 2003; Helz et al. 2011), but must also reflect differences in dU. These may include distinct microbial processes removing dU within the redox transition zone in Lake Poso as well as less kinetic stabilization of dU reduction (e.g., Hua et al. 2006) due to lower pH (≈ 7, Kaban et al. 2023) and $[CO_3^{2-}]$ (Damanik et al. 2023) in Lake Poso compared to marine basins.

A biological role for reductive trace element removal

The profile of dSe in Lake Poso shows two separated horizons of removal—first decreasing in the oxycline and reaching stable values above the metal oxide zone. The former corresponds with observed TDN and dU behavior, within the deep euphotic zone, indicating a microbially driven mechanism shaping both dU and dSe distributions (Fig. 2). Similar removal of oxidized Se species (Se(VI)) has been observed at the surface of oligotrophic lakes (Bueno et al. 2022) or above the oxic–anoxic interface in the Black Sea (Cutter 1992), due to phytoplankton uptake, assimilatory reduction and/or dissimilatory microbial reduction to more easily scavenged reduced Se species (Se(IV), organic Se, or Se(0) nanoparticles). Because dissimilatory Se reduction is inhibited by oxidized Mn (e.g., Oremland 1994), and the formation of Se(IV) would be followed by a Se removal at the metal oxide zone (e.g., Fernández-Martínez and Charlet 2009), which is not observed (Supporting Information Fig. S3), oxic zone Se removal likely reflects assimilation of Se into biota and/or assimilatory reduction into organic Se species or particulate Se(0). Within the anoxic zone, dSe decreases with SO_4^{2-} and dMo, thus contrasting the deep-water Se accumulation (as organic Se species) observed in euxinic waters (Cutter 1992). The dSe decrease in the anoxic Lake Poso hypolimnion suggests a sediment removal term for dSe, likely through dissimilatory biotic or abiotic Se reduction into elemental Se (nano)particles or metal selenides, as reported in reducing sediments (Oremland 1994). It also indicates minimal Se release from sinking particulate phases, which likely contain organoselenium compounds from biotic assimilation in overlying waters, in contrast to many other trace elements. Further study incorporating Se speciation would help to clarify the specific processes acting to remove dSe.

Comparison of trace element distributions across ferruginous systems

General characteristics

Ferruginous waters represent a major geochemical state throughout Earth's history (Planavsky et al. 2011; Poulton and Canfield 2011; Swanner et al. 2020). To constrain broad

19395590, 2024, 11, Downloaded from https://aslopubs.onlinelibrary.wiley.com/doi/10.1002/lno.12687 by Paul Scherrer Institut PSI, Wiley Online Library on [02/12/2024]. See the Terms and Conditions (https://onlinelibrary.wiley.com/terms-and-conditions) on Wiley Online Library for rules of use; OA articles are governed by the applicable Creative Commons License

expectations of biogeochemical cycling in ferruginous waters and interpret trace element records in ferruginous sediments, it is necessary to differentiate local controls from generalizable geochemical trends. This requires compiling data across diverse systems; however, trace element data are sparse in modern ferruginous basins. Here we compare trace element data in diverse ferruginous lakes to disentangle local, basin-specific processes from generalizable trends. In addition to Lake Poso, the deep lakes with available data are Lake Matano (Indonesia, Crowe et al. 2008) and Lake Pavin (France, Viollier et al. 1995). Data are also available from small, shallow meso- and eutrophic lakes, including Hall Lake (USA, Balistrieri et al. 1994), and for some trace metals Brownie and Canyon Lakes (USA) (Lambrecht et al., 2018; Cole et al., 2020). This comparison indicates Lake Poso should serve as a useful analog system to understand biogeochemical cycling and paleoproxy behavior in Earth's ferruginous paleoceans.

Details on physical and geochemical conditions of the other ferruginous lakes are given in the study site description and in Supporting Information Table S2. As discussed above, maximum dFe accumulation is smaller in Lake Poso than previously studied deep ($Z_{max} > 90$ m) ferruginous systems, while SO_4^{2-} removal occurs deeper and is less complete than in some other lakes (Supporting Information Table S3). Similarly, dFe gradients and dFe_{max} are lower in Lake Poso than in smaller, shallow systems, likely due to sharper pycnoclines, sediment proximity and elevated anoxic electron acceptor demand in shallow ($Z_{max} < 30$ m) mesotrophic and eutrophic systems (Brownie, Canyon, Hall; Balistrieri et al. 1994; Lambrecht et al., 2018).

The distributions of most trace elements in Lake Pavin (deep waters) and Lake Matano (surface waters) strongly contrast those in other ferruginous lakes (Fig. 4; Supporting Information Fig. S7; Table S3). In anoxic deep waters of Lake Pavin, trace element concentrations are orders of magnitude higher than in oxic waters, likely reflecting an input of trace element-rich deep waters. Similarly, concentrations in surface waters Lake Matano are orders of magnitude higher than in other ferruginous systems, reflecting the metal-rich catchment and potential impacts from nearby mining. These highlight the two environments as geochemically distinct, with possible deviation from other anoxic sites through space and time. Therefore, use of these systems as analog environments should include consideration that the processes targeted reflect their underlying ferruginous nature and not the local deviations.

Water column distributions of individual trace elements

While dCr ranges vary between individual systems based on local controls (Cr-rich surface water, close proximity to sediments, potential subsurface input), redox interface dCr removal is always incomplete, and Cr concentrations increase in ferruginous waters relative to the interface (Fig. 4a,g; Supporting Information Table S3; this study; Balistrieri et al. 1994; Viollier et al. 1995; Crowe et al. 2008; Lambrecht et al. 2018). This is consistent with trends in ferruginous sediments (Bauer et al. 2018) and in euxinic waters (Janssen et al. 2022), suggesting the behavior is generalizable across anoxic systems (both marine and freshwater)—all available water column data indicate nonquantitative Cr removal and often Cr increases in anoxic water. This contrasts widely applied assumptions of efficient, near-quantitative Cr reduction and removal across oxic–anoxic interfaces in paleoreconstructions (Reinhard et al. 2014; Swanner et al. 2020; Wei et al. 2020). Dissolved V resembles dCr across the diverse ferruginous systems, reflecting the geochemical similarity of these elements (e.g., Balistrieri et al. 1994) and supporting the same generalizable features—nonquantitative removal at the oxic–anoxic interface and accumulation of dV in ferruginous deep waters (Fig. 4c,i).

Nickel data show a local minimum near but above the oxic–anoxic interface at some sites (Fig. 4b, h; Poso and Matano; this study; Crowe et al. 2008). Concentrations generally increase below the interface, with maximum Ni concentrations in the upper anoxic zone in lakes Poso, Matano, and Hall (Balistrieri et al. 1994), reflecting the shallow dissolution of Ni-bearing MnOx phases. Nickel concentrations then decrease in deeper waters, with dNi minima related to water column H_2S maxima (Balistrieri et al. 1994; Crowe et al. 2008), green rust formation (Zegeye et al. 2012) or proximity to sediments (this study; Viollier et al. 1995), indicating removal may be more prevalent in the sediments than the water column in some settings. Interestingly, this strong decrease in dNi is less apparent in euxinic basins (e.g., Jacobs and Emerson 1982; Vance et al. 2016), despite orders of magnitude higher H_2S concentrations. This may reflect high deep-water sources relative to sinks in marine settings (Little et al. 2015) but not in ferruginous lakes, other mechanisms acting to stabilize dNi in marine basins, or that removal is not necessarily H_2S-driven. Given the role of Ni in anaerobic metabolism (i.e., methanogenesis, Robbins et al. 2016), and the potential importance of Ni availability through time in ferruginous settings (e.g., Konhauser et al. 2009), future investigation of the roles and removal mechanisms of Ni in ferruginous deep waters is warranted. Finally, Lake Matano shows a sharp decrease in dNi concentration just below the oxic-anoxic interface, attributed to Ni scavenging onto green rust (Zegeye et al. 2012). This is not seen in the other lakes (Fig. 4), and therefore may not be a generalizable feature of ferruginous settings. Dissolved Co behaves similarly to prior ferruginous data, reflecting control by Mn oxides and accumulation at the top of the anoxic zone following MnOx reduction (Viollier et al. 1995; Lienemann et al. 1997; Taillefert et al. 2002; Crowe et al. 2008), but without the stronger deep-water dNi minimum. Mild minima in some but not all ferruginous sites suggest dCo distributions are sensitive to the potential formation of mixed sulfide species (e.g., Swanner et al. 2014), and therefore may show smaller scale site-specific dependencies.

Dissolved U data are broadly similar among anoxic sites—lower dU concentrations are reported in euxinic (e.g., Black

19395590, 2024, 11, Downloaded from https://aslopubs.onlinelibrary.wiley.com/doi/10.1002/lno.12687 by Paul Scherrer Institut PSI, Wiley Online Library on [02/12/2024]. See the Terms and Conditions (https://onlinelibrary.wiley.com/terms-and-conditions) on Wiley Online Library for rules of use; OA articles are governed by the applicable Creative Commons License

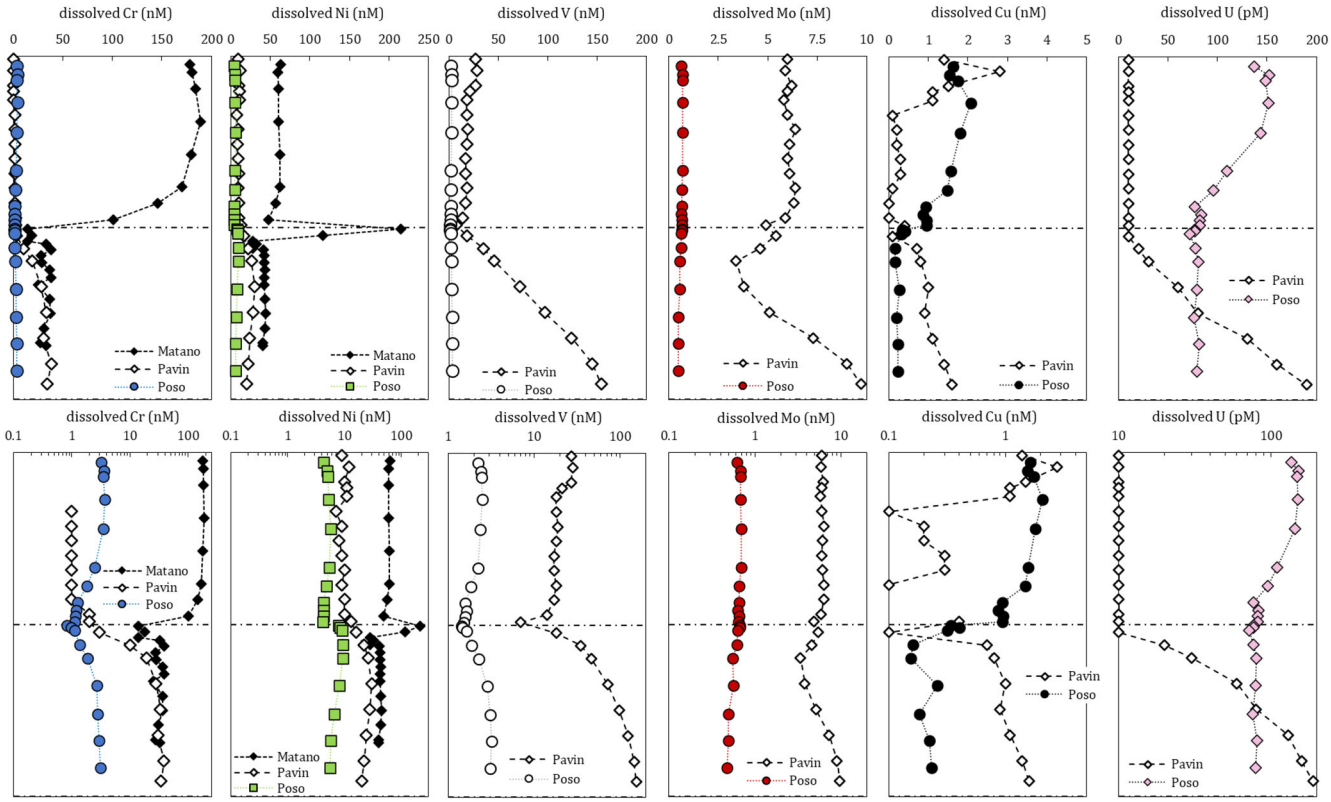

Fig. 4. Comparison of trace element distributions across ferruginous systems. Data are compared with a linear scale (top) and a logarithmic scale (bottom). The vertical axis is a scaled depth parameter, from lake surface (top) to sediments (bottom), with the redox interface in the middle. Note that most of the Lake Matano Cr data at and below the redox interface are below the detection limit (30 nM). *Source*: Lake Poso: this study; Lake Matano: Crowe et al. (2008); Lake Pavin: Viollier et al. (1995); Brownie Lake: Cole et al. (2020). See also Supporting Information Fig. S7.

Sea: Colodner et al. 1995), and ferruginous (Brownie Lake: Cole et al., 2020; Fig. 4f,l) waters. However, the exact locations and subsequent mechanisms of dU removal differ considerably. Prior data show dU minima are reached within the anoxic zone rather than above it, with dU distributions instead explained by reductive removal in surface sediments (Colodner et al. 1995; Lau et al. 2019). Dissolved U in Lake Poso is inconsistent with sediment-based controls as gradients are only observed within the oxycline, with subsequent stable dU across the oxic–anoxic interface and until the sediments. Consequently, while dU deficits in the anoxic Lake Poso hypolimnion supports enhanced sedimentary U accumulation through removal from the water column, as applied in U-based anoxia paleoreconstructions (Lau et al. 2019), mechanistic controls differ among anoxic settings, and water column rather than sediment processes may regulate dU in some basins. Differing stabilization of oxidized U species by carbonate complexation (Hua et al. 2006) may play a role in the diverse U behavior across these settings.

Despite the interest in Se and its stable isotopes as sensitive paleoredox tracers, especially in the ferruginous paleocean (e.g., Wen et al. 2014), these are the first dSe data from ferruginous waters. The presence of two distinct removal zones—within the lower oxycline and in sediments—indicates distinct removal processes, likely microbial reduction and/or uptake in the lower oxycline, and biotic or abiotic reduction in sediments. This suggests that sediment records would likely reflect at least two distinct pools of authigenic Se, and therefore potentially distinct isotope fractionations from distinct dSe reservoirs, which might complicate paleoreconstructions. Future study is needed in modern environments, including Se speciation and stable isotope composition.

With the present data, it is difficult to draw clear generalizable conclusions about Mo and Cu. Despite experimental data of Mo adsorption onto metal oxides and their importance in the modern ocean Mo budget (e.g., Goldberg et al. 2009), and despite ocean sediment studies suggesting Mo delivery by sinking oxides (e.g., Scholz et al., 2013), there is little to no evidence of Mo removal onto oxides in the available ferruginous lake data (Fig. 4d,j). Instead, in ferruginous waters, Mo removal may primarily be dictated by sulfide availability, either in the water column (Pavin: Viollier et al. 1995) or sediments (Poso: this study; Hall: Balistrieri et al. 1994), which is system dependent. Given the very low solubility of CuS, Cu should be removed at H_2S levels well below detection limits. However, dCu persists in some ferruginous systems (Fig. 4e,k)

19395590, 2024, 11, Downloaded from https://aslopubs.onlinelibrary.wiley.com/doi/10.1002/lno.12687 by Paul Scherrer Institut PSI, Wiley Online Library on [02/12/2024]. See the Terms and Conditions (https://onlinelibrary.wiley.com/terms-and-conditions) on Wiley Online Library for rules of use; OA articles are governed by the applicable Creative Commons License

despite μM-level H_2S (e.g., Hall: Balistrieri et al. 1994; Pavin: Viollier et al. 1995) and is removed nearly completely in Lake Poso without such levels. Therefore, differences may reflect other system-specific parameters such as stabilization with organic matter or colloids in eutrophic lakes, and/or deep Cu sources (in Lake Pavin). This contrast among modern ferruginous basins indicates more constraints are needed to assess the reliability of low Cu availability modeled throughout the ferruginous paleocean (cf Robbins et al. 2016). Dissolved Cu may also be removed onto oxide phases at the redox interface (this study), though this may be masked by stronger responses to H_2S and poor spatial separation of metal oxide formation and H_2S accumulation in other systems (e.g., Hall: Balistrieri et al. 1994; Pavin: Viollier et al. 1995), and the overall removal mechanism remains poorly constrained.

Conclusions

Ancient Lake Poso (Indonesia) is one of the world's largest known ferruginous lakes. Trace element distributions are largely driven by the major redox transitions across the oxic–anoxic interface (~ 90 m depth), and distinct processes along this redox transition more easily differentiated based on their spatial separation (Fig. 5) compared to many previously studied environments. Manganese cycling acts as a primary control on dCo and dNi, with dissolved minima in the zone of MnOx formation, sharp increases directly below this zone, and with mid-depth maxima in anoxic waters. Decreasing dNi and, to a lesser extent, dCo in the deepest samples reflect removal to sediments, possibly as sulfide phases. Dissolved V, dCr, TDP, and dAs show smoothly increasing concentrations within the anoxic zone and maxima in the deepest samples, reflecting control by Fe. Absolute local minima of dV and dCr are seen coincident with the particulate Fe peak, and stable low concentrations of TDP and dAs above the metal oxide zone indicate efficient retention in the hypolimnion. Dissolved Cu and dCd, both especially sensitive to trace levels of H_2S, are nearly completely removed from the water column by the upper anoxic zone, with Fe and Mn oxides potentially active in the overall removal process. Removal of dU occurs

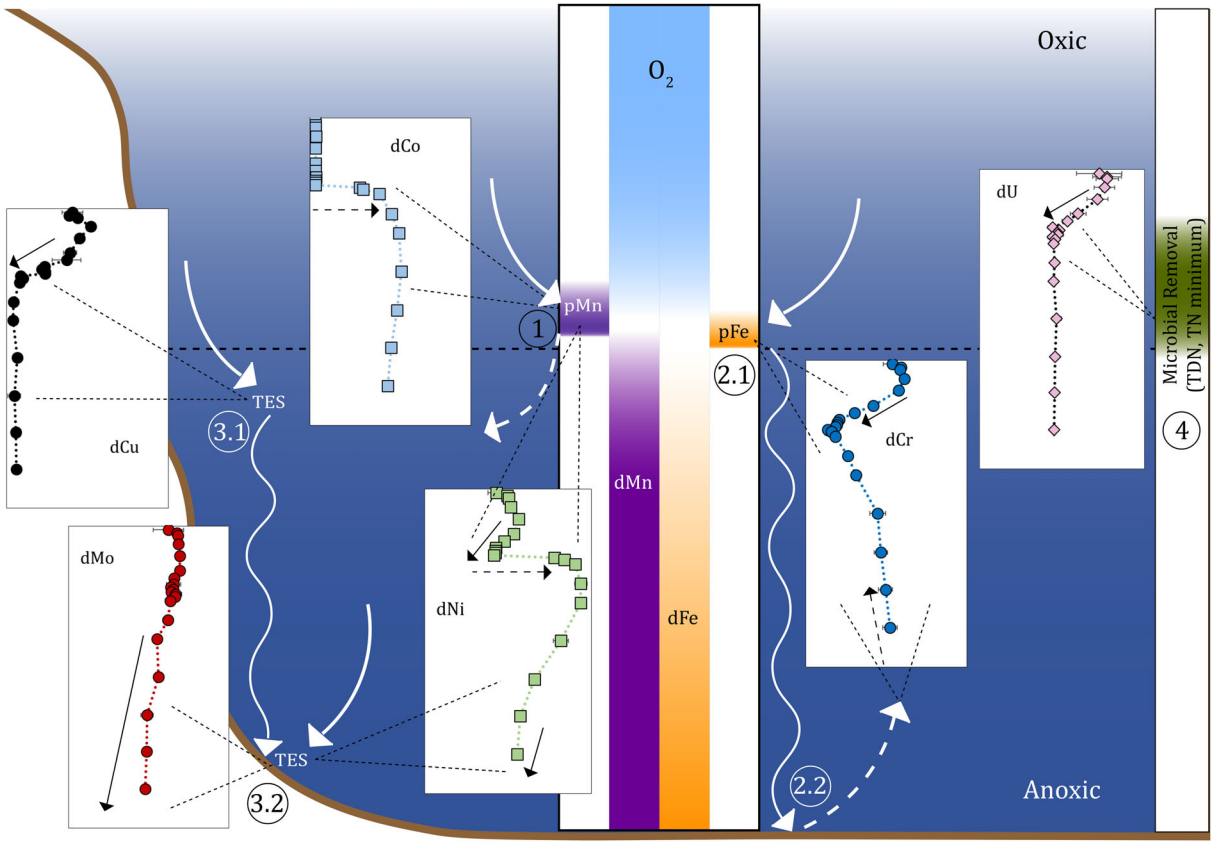

Fig. 5. Conceptual schematic of processes shaping trace element distributions. Major gradients of O_2, Fe, and Mn are shown against a schematic of Lake Poso, divided into oxic and anoxic zones. Key processes controlling element distribution are highlighted by specific depth profiles. Solid arrows show transfer from dissolved to solid phases, dashed arrows show transfer from solid to dissolved phases, and curved lines indicate sinking particles. (1) Particulate MnOx form and scavenge dissolved metals, with reductive dissolution in the upper anoxic zone releasing dissolved metals. (2) Particulate FeOx form (2.1) and sink to sediments, where reductive dissolution releases metals back to the water column (2.2). (3) Trace element sulfides (TES) form, either in the water column for especially insoluble sulfides (3.1) or in the sediments (3.2). (4) Microbial removal, via biological reduction to insoluble forms and/or uptake, within the lower oxycline.

19395590, 2024, 11, Downloaded from https://aslopubs.onlinelibrary.wiley.com/doi/10.1002/lno.12687 by Paul Scherrer Institut PSI, Wiley Online Library on [02/12/2024]. See the Terms and Conditions (https://onlinelibrary.wiley.com/terms-and-conditions) on Wiley Online Library for rules of use; OA articles are governed by the applicable Creative Commons License

mainly in the water column, at the base of the oxycline, while SO_4^{2-} and Mo removal is mostly in sediments, and with dSe removed in both settings. Both dSe and dU profiles are consistent with active biological reduction and/or uptake, with removal horizons coincident with the TDN minimum. Anoxic zone dRe concentrations are lower than those in the oxic zone, though dRe removal is relatively minor.

By comparison with other ferruginous systems, data from Lake Poso help establish a set of generalizable expectations, as well as identify site-specific deviations driven by local controls. The high heterogeneity among lakes underscores the importance of considering local controlling factors and the choice of system for specific questions. Generally, hypolimnion dCu, dMo, dCd, and dU concentrations are lower than the epilimnion, unless major deep-water sources are present (e.g., Lake Pavin). The extent and location of dMo removal depends on H_2S, and therefore varies qualitatively and quantitatively between ferruginous settings. Nickel is nonquantitatively removed at the redox interface. Both dNi and dCo increase in anoxic waters and then are removed in sediments or deep waters. This may be as sulfides, though contrasts between dNi distributions in ferruginous lakes and euxinic settings indicate remaining uncertainties in dNi cycling. Both dV and dCr are also nonquantitatively removed at the oxic–anoxic interface and accumulate in anoxic deep waters, indicating their removal to sediments is inefficient despite anoxia. This contrasts Cr-based paleoproxy assumptions and indicates the need to revise interpretive frameworks in paleoreconstructions. The first ferruginous dSe data show two removal horizons, indicating sediment records should reflect at least two distinct sources of Se to sediments. Mechanisms and isotope fractionations controlling these processes would help to refine paleoreconstructions based on Se. Contrasts in dMo, dRe, and dU behavior between ferruginous and euxinic basins indicates potential for combined utility of these tracers to differentiate removal mechanisms and paleoredox.

Lake Poso also shows strong potential as a site for paleoreconstructions. Physical stratification is weaker than other tropical anoxic lakes and almost entirely driven by temperature, indicating that lake mixing would be especially sensitive to climate (i.e., drivers of surface cooling, such as enhanced evaporation). The limited anthropogenic pressures and oligotrophic surface conditions, clear trace element gradients across the oxic–anoxic interface, and nutrient-rich deep waters indicate enhanced mixing should drive changes in biogeochemical cycling, and subsequently influence the sediment record. Lake Poso is therefore a promising site for future study, serving as an analog of biogeochemical cycling in the early Earth where in situ biogeochemical cycling can be better isolated in a natural setting based on the separation of redox fronts (e.g., Mn, Fe, and S reduction), and where sediment archives may serve as sensitive paleoclimate records. The dynamic water column distributions of redox-active elements (e.g., Se, U) also highlights potential for research on the in situ cycling of these elements, including mechanisms, associated isotope fractionations and sediment signals.

Data availability statement

All new trace element, major ion, nutrient, and CTD data discussed in this manuscript are presented in tables in the Supporting Information and as an open-access dataset in Zenodo (10.5281/zenodo.13141073).

References

Aeschbach-Hertig, W., M. Hofer, M. Schmid, R. Kipfer, and D. M. Imboden. 2002. The physical structure and dynamics of a deep, meromictic crater lake (Lac Pavin, France). Hydrobiologia **487**: 111–136. doi:10.1023/A:1022942226198

Albrecht, C., B. Stelbrink, P. Gauffre-Autelin, R. M. Marwoto, T. von Rintelen, and M. Glaubrecht. 2020. Diversification of epizoic freshwater limpets in ancient lakes on Sulawesi, Indonesia: Coincidence or coevolution? J. Great Lakes Res. **46**: 1187–1198. doi:10.1016/j.jglr.2020.07.013

Aldrian, E., and R. Dwi Susanto. 2003. Identification of three dominant rainfall regions within Indonesia and their relationship to sea surface temperature. Int. J. Climatol. **23**: 1435–1452. doi:10.1002/joc.950

Balistrieri, L. S., J. W. Murray, and B. Paul. 1994. The geochemical cycling of trace elements in a biogenic meromictic lake. Geochim. Cosmochim. Acta **58**: 3993–4008. doi:10.1016/0016-7037(94)90262-3

Bauer, K. W., B. Gueguen, D. B. Cole, R. Francois, J. Kallmeyer, B. N. Planavsky, and S. A. Crowe. 2018. Chromium isotope fractionation in ferruginous sediments. Geochim. Cosmochim. Acta **223**: 198–215. doi:10.1016/j.gca.2017.10.034

Bennett, W. W., and D. E. Canfield. 2020. Redox-sensitive trace metals as paleoredox proxies: A review and analysis of data from modern sediments. Earth Sci. Rev. **204**: 103175. doi:10.1016/j.earscirev.2020.103175

Brennecka, G. A., L. E. Wasylenki, J. R. Bargar, S. Weyer, and A. D. Anbar. 2011. Uranium isotope fractionation during adsorption to Mn-oxyhydroxides. Environ. Sci. Technol. **45**: 1370–1375. doi:10.1021/es103061v

Bueno, M., B. Duval, E. Tessier, A. Romero-Rama, L. Kortazar, L. Á. Fernández, A. de Diego, and D. Amouroux. 2022. Selenium distribution and speciation in waters of pristine alpine lakes from central-western Pyrenees (France–Spain). Environ Sci Process Impacts **24**: 1430–1442. doi:10.1039/D1EM00430A

Busigny, V., and others. 2016. The iron wheel in Lac Pavin: Interaction with phosphorus cycle, p. 205–220. *In* T. Sime-Ngando, P. Boivin, E. Chapron, D. Jezequel, and M. Meybeck [eds.], Lake Pavin. Springer. doi:10.1007/978-3-319-39961-4_12

19395590, 2024, 11, Downloaded from https://aslopubs.onlinelibrary.wiley.com/doi/10.1002/lno.12687 by Paul Scherrer Institut PSI, Wiley Online Library on [02/12/2024]. See the Terms and Conditions (https://onlinelibrary.wiley.com/terms-and-conditions) on Wiley Online Library for rules of use; OA articles are governed by the applicable Creative Commons License

Canfield, D. E., and B. O. Thamdrup. 2009. Towards a consistent classification scheme for geochemical environments, or, why we wish the term "suboxic" would go away. Geobiology **7**: 385–392. doi:10.1111/j.1472-4669.2009.00214.x

Carey, C. C., and others. 2022. Anoxia decreases the magnitude of the carbon, nitrogen, and phosphorus sink in freshwaters. Glob. Chang. Biol. **28**: 4861–4881. doi:10.1111/gcb.16228

Cole, D. B., N. J. Planavsky, M. Longley, P. Böning, D. Wilkes, X. Wang, E. D. Swanner, C. Wittkop, D. K. Loydell, V. Busigny, and A. C. Knudsen. 2020. Uranium isotope fractionation in non-sulfidic anoxic settings and the global uranium isotope mass balance. Glob Biogeochem Cy. **34**: e2020GB006649. doi:10.1029/2020GB006649

Colodner, D., J. Edmond, and E. Boyle. 1995. Rhenium in the Black Sea: Comparison with molybdenum and uranium. Earth Planet. Sci. Lett. **131**: 1–15. doi:10.1016/0012-821X(95)00010-A

Coon, T. G., M. M. Lopez, P. J. Richerson, T. M. Powell, and C. R. Goldman. 1987. Summer dynamics of the deep chlorophyll maximum in Lake Tahoe. J. Plankton Res. **9**: 327–344. doi:10.1093/plankt/9.2.327

Crowe, S. A., A. H. O'Neill, S. Katsev, P. Hehanussa, G. D. Haffner, B. Sundby, A. Mucci, and D. A. Fowle. 2008. The biogeochemistry of tropical lakes: A case study from Lake Matano, Indonesia. Limnol. Oceanogr. **53**: 319–331. doi:10.4319/lo.2008.53.1.0319

Cutter, G. A. 1992. Kinetic controls on metalloid speciation in seawater. Mar. Chem. **40**: 65–80. doi:10.1016/0304-4203(92)90048-F

Dahl, T. W., A. D. Anbar, G. W. Gordon, M. T. Rosing, R. Frei, D. E. Canfield. 2010. The behavior of molybdenum and its isotopes across the chemocline and in thesediments of sulfidic Lake Cadagno, Switzerland. Geochim. Cosmochim. Act. **74**: 144-163. doi:10.1016/j.gca.2009.09.018

Damanik, A., D. J. Janssen, N. Tournier, B. Stelbrink, T. von Rintelen, G. D. Haffner, A. Cohen, S. Y. Cahyarini, and H. Vogel. 2023. Perspectives from modern hydrology and hydrochemistry on a lacustrine biodiversity hotspot: Ancient Lake Poso, Central Sulawesi, Indonesia. J. Great Lakes Res. **50**: 102254. doi:10.1016/j.jglr.2023.102254

Davison, W. 1993. Iron and manganese in lakes. Earth Sci. Rev. **34**: 119–163. doi:10.1016/0012-8252(93)90029-7

Dellwig, O., T. Leipe, C. März, M. Glockzin, F. Pollehne, B. Schnetger, E. V. Yakushev, M. E. Böttcher, and H. J. Brumsack. 2010. A new particulate Mn–Fe–P-shuttle at the redoxcline of anoxic basins. Geochim. Cosmochim. Acta **74**: 7100–7115. doi:10.1016/j.gca.2010.09.017

Fernández-Martínez, A., and L. Charlet. 2009. Selenium environmental cycling and bioavailability: A structural chemist point of view. Rev. Environ. Sci. Biotechnol. **8**: 81–110. doi:10.1007/s11157-009-9145-3

Fukushima, T., B. Matsushita, L. Subehi, F. Setiawan, and H. Wibowo. 2017. Will hypolimnetic waters become anoxic in all deep tropical lakes? Sci. Rep. **7**: 45320. doi:10.1038/srep45320

Gaillardet, J., J. Viers, and B. Dupré. 2014, p. 195–235. *In* H. D. Holland and K. K. Turekian [eds.], Trace elements in river waters. In treatise on geochemistry, 2nd ed. Elsevier. doi:10.1016/B978-0-08-095975-7.00507-6

GEOTRACES Intermediate Data Product Group. 2021. The GEOTRACES Intermediate Data Product 2021 (IDP2021). NERC EDS British Oceanographic Data Centre NOC. doi:10.5285/cf2d9ba9-d51d-3b7c-e053-8486abc0f5fd

Goldberg, T., C. Archer, D. Vance, and S. W. Poulton. 2009. Mo isotope fractionation during adsorption to Fe (oxyhydr) oxides. Geochim. Cosmochim. Acta **73**: 6502–6516. doi:10.1016/j.gca.2009.08.004

Hampton, S. E., and others. 2018. Recent ecological change in ancient lakes. Limnol. Oceanogr. **63**: 2277–2304. doi:10.1002/lno.10938

Helz, G. R., E. Bura-Nakić, N. Mikac, and I. Ciglenečki. 2011. New model for molybdenum behavior in euxinic waters. Chem. Geol. **284**: 323–332. doi:10.1016/j.chemgeo.2011.03.012

Hidayat, H. 2019. Trend of rainfall over Indonesian major lakes from tropical rainfall measuring mission data. IOP Conf. Ser. Earth Environ. Sci. **303**: 012019. doi:10.1088/1755-1315/303/1/012019

Horner, T. J., and others. 2021. Bioactive trace metals and their isotopes as paleoproductivity proxies: An assessment using GEOTRACES-era data. Global Biogeochem. Cycles **35**: e2020GB006814. doi:10.1029/2020GB006814

Hua, B., H. Xu, J. Terry, and B. Deng. 2006. Kinetics of uranium (VI) reduction by hydrogen sulfide in anoxic aqueous systems. Environ. Sci. Technol. **40**: 4666–4671. doi:10.1021/es051804n

Jacobs, L., and S. Emerson. 1982. Trace metal solubility in an anoxic fjord. Earth Planet. Sci. Lett. **60**: 237–252. doi:10.1016/0012-821X(82)90006-1

Jane, S. F., J. L. Mincer, M. P. Lau, A. S. Lewis, J. T. Stetler, and K. C. Rose. 2023. Longer duration of seasonal stratification contributes to widespread increases in lake hypoxia and anoxia. Glob. Chang. Biol. **29**: 1009–1023. doi:10.1111/gcb.16525

Janssen, D. J., and others. 2022. Chromium cycling in redox-stratified basins challenges δ^{53}Cr paleoredox proxy applications. Geophys. Res. Lett. **49**: e2022GL099154. doi:10.1029/2022GL099154

Jones, C., S. A. Crowe, A. Sturm, K. L. Leslie, L. C. W. MacLean, S. Katsev, C. Henny, D. A. Fowle, and D. E. Canfield. 2011. Biogeochemistry of manganese in ferruginous Lake Matano, Indonesia. Biogeosciences **8**: 2977–2991. doi:10.5194/bg-8-2977-2011

Kaban, S., Y. C. Ditya, and K. F. Safran Makmur. 2023. Water quality and trophic status to estimate fish production potential for sustainable fisheries in Lake Poso, Central Sulawesi. Pol. J. Environ. Stud. **32**: 4083–4093. doi:10.15244/pjoes/168102

19395590, 2024, 11, Downloaded from https://aslopubs.onlinelibrary.wiley.com/doi/10.1002/lno.12687 by Paul Scherrer Institut PSI, Wiley Online Library on [02/12/2024]. See the Terms and Conditions (https://onlinelibrary.wiley.com/terms-and-conditions) on Wiley Online Library for rules of use; OA articles are governed by the applicable Creative Commons License

Katsev, S., S. A. Crowe, A. Mucci, B. Sundby, S. Nomosatryo, G. Douglas Haffner, and D. A. Fowle. 2010. Mixing and its effects on biogeochemistry in the persistently stratified, deep, tropical Lake Matano, Indonesia. Limnol. Oceanogr. **55**: 763–776. doi:10.4319/lo.2010.55.2.0763

Katsev, S., P. Verburg, M. Llirós, E. C. Minor, B. R. Kruger, and J. Li. 2017. Tropical meromictic lakes: Specifics of meromixis and case studies of lakes Tanganyika, Malawi, and Matano. *In* R. Gulati, E. Zadereev, and A. Degermendzhi [eds.], Ecology of meromictic Lakes. Ecological studies, v. **228**. Springer. doi:10.1007/978-3-319-49143-1_10

Konhauser, K. O., E. Pecoits, S. V. Lalonde, D. Papineau, E. G. Nisbet, M. E. Barley, N. T. Arndt, K. Zahnle, and B. S. Kamber. 2009. Oceanic nickel depletion and a methanogen famine before the Great Oxidation Event. Nature **458**: 750–753. doi:10.1038/nature07858

Koschinsky, A., and J. R. Hein. 2003. Uptake of elements from seawater by ferromanganese crusts: Solid-phase associations and seawater speciation. Mar. Geol. **198**: 331–351. doi:10.1016/S0025-3227(03)00122-1

Lambrecht, N., C. Wittkop, S. Katsev, M. Fakhraee, and E. D. Swanner. 2018. Geochemical characterization of two ferruginous meromictic lakes in the Upper Midwest, USA. J. Geophys. Res. **123**: 3403-3422. doi:10.1029/2018JG004587

Lau, K. V., S. J. Romaniello, and F. Zhang. 2019. The uranium isotope paleoredox proxy. Cambridge Univ. Press. doi:10.1017/9781108584142

Lee, Z., S. Shang, K. Du, and J. Wie. 2018. Resolving the long-standing puzzles about the observed depth Secchi depth relationships. Limnol. Oceanogr. **63**: 2321–2336. doi:10.1002/lno.10940

Lehmusluoto, P., Machbub, B., Terangna, N., Rusmiputro, S., Achmad, F., Boer, L., Brahmana, S.S., Priadi, B., Setiadji, B., Sayuman, O., Margana, A. (1997). National inventory of the major lakes and reservoirs in Indonesia. Expedition Indodanau technical report. Edita Oy.

Lienemann, C. P., M. Taillefert, D. Perret, and J. F. Gaillard. 1997. Association of cobalt and manganese in aquatic systems: Chemical and microscopic evidence. Geochim. Cosmochim. Acta **61**: 1437–1446. doi:10.1016/S0016-7037(97)00015-X

Little, S. H., D. Vance, T. W. Lyons, and J. McManus. 2015. Controls on trace metal authigenic enrichment in reducing sediments: Insights from modern oxygen-deficient settings. Am. J. Sci. **315**: 77–119. doi:10.2475/02.2015.01

Meyer, K. M., and L. R. Kump. 2008. Oceanic euxinia in earth history: Causes and consequences. Annu. Rev. Earth Planet. Sci. **36**: 251–288. doi:10.1146/annurev.earth.36.031207.124256

Michard, G., E. Viollier, D. Jézéquel, and G. Sarazin. 1994. Geochemical study of a crater lake: Pavin Lake, France—identification, location and quantification of the chemical reactions in the lake. Chem. Geol. **115**: 103–115. doi:10.1016/0009-2541(94)90147-3

Naqvi, S. W., H. W. Bange, L. Farías, P. M. Monteiro, M. I. Scranton, and J. Zhang. 2010. Marine hypoxia/anoxia as a source of CH_4 and N_2O. Biogeosciences **7**: 2159–2190. doi:10.5194/bg-7-2159-2010

Oremland, R. S. 1994. Biogeochemical transformations of selenium in anoxic environments, p. 389–419. *In* W. T. Frankenberger Jr. and S. Benson [eds.], Selenium in the environment. CRC Press. doi:10.1201/9781482293432

Planavsky, N. J., and others. 2011. Widespread iron-rich conditions in the mid-Proterozoic ocean. Nature **477**: 448–451. doi:10.1038/nature10327

Poulton, S. W., and D. E. Canfield. 2011. Ferruginous conditions: A dominant feature of the ocean through Earth's history. Elements **7**: 107–112. doi:10.2113/gselements.7.2.107

Reinhard, C. T., N. J. Planavsky, X. Wang, W. W. Fischer, T. M. Johnson, and T. W. Lyons. 2014. The isotopic composition of authigenic chromium in anoxic marine sediments: A case study from the Cariaco Basin. Earth Planet. Sci. Lett. **407**: 9–18. doi:10.1016/j.epsl.2014.09.024

Robbins, L. J., and others. 2016. Trace elements at the intersection of marine biological and geochemical evolution. Earth Sci. Rev. **163**: 323–348. doi:10.1016/j.earscirev.2016.10.013

Rue, E. L., G. J. Smith, G. A. Cutter, and K. W. Bruland. 1997. The response of trace element redox couples to suboxic conditions in the water column. Deep-Sea Res. I. Oceanogr. Res. Pap. **44**: 113–134. doi:10.1016/S0967-0637(96)00088-X

Sabo, E., D. Roy, P. B. Hamilton, P. E. Hehanussa, R. McNeely, and D. G. Haffner. 2009. The plankton community of Lake Matano: Factors regulating plankton composition and relative abundance in an ancient, tropical lake of Indonesia, p. 225–235. *In* Patterns and processes of speciation in Ancient Lakes: Proceedings of the Fourth Symposium on Speciation in Ancient Lakes, Berlin, Germany, September 4–8, 2006. Springer. doi:10.1007/978-1-4020-9582-5_16

Schmidtko, S., L. Stramma, and M. Visbeck. 2017. Decline in global oceanic oxygen content during the past five decades. Nature **542**: 335–339. doi:10.1038/nature21399

Sulawesty, F., H. Triyanto, G. Lukman, O. Samir, F. Ali, and E. Nafisyah. 2022. Trophic status of waters in poso watershed, Central Sulawesi. IOP Conf. Ser. Earth Environ. Sci. **950**: 012039. doi:10.1088/1755-1315/950/1/012039

Swanner, E. D., N. Lambrecht, C. Wittkop, C. Harding, S. Katsev, J. Torgeson, and S. W. Poulton. 2020. The biogeochemistry of ferruginous lakes and past ferruginous oceans. Earth Sci. Rev. **211**: 103430. doi:10.1016/j.earscirev.2020.103430

Swanner, E. D., and others. 2014. Cobalt and marine redox evolution. Earth Planet. Sci. Lett. **390**: 253–263. doi:10.1016/j.epsl.2014.01.001

Taillefert, M., B. J. MacGregor, J. F. Gaillard, C. P. Lienemann, D. Perret, and D. A. Stahl. 2002. Evidence for a dynamic cycle between Mn and Co in the water column of a

19395590, 2024, 11, Downloaded from https://aslopubs.onlinelibrary.wiley.com/doi/10.1002/lno.12687 by Paul Scherrer Institut PSI, Wiley Online Library on [02/12/2024]. See the Terms and Conditions (https://onlinelibrary.wiley.com/terms-and-conditions) on Wiley Online Library for rules of use; OA articles are governed by the applicable Creative Commons License

stratified lake. Environ. Sci. Technol. **36**: 468–476. doi:10.1021/es010915t

Teutsch, N., M. Schmid, B. Müller, A. N. Halliday, H. Bürgmann, and B. Wehrli. 2009. Large iron isotope fractionation at the oxic–anoxic boundary in Lake Nyos. Earth Planet. Sci. Lett. **285**: 52–60. doi:10.1016/j.epsl.2009.05.044

Tribovillard, N., T. J. Algeo, T. Lyons, and A. Riboulleau. 2006. Trace metals as paleoredox and paleoproductivity proxies: An update. Chem. Geol. **232**: 12–32. doi:10.1016/j.chemgeo.2006.02.012

Vaillant, J. J., G. D. Haffner, and M. E. Cristescu. 2011. The ancient lakes of Indonesia: Towards integrated research on speciation. Integr. Comp. Biol. **51**: 634–643. doi:10.1093/icb/icr101

Van Cappellen, P., and E. D. Ingall. 1994. Benthic phosphorus regeneration, net primary production, and ocean anoxia: A model of the coupled marine biogeochemical cycles of carbon and phosphorus. Paleoceanography **9**: 677–692. doi:10.1029/94PA01455

Vance, D., S. H. Little, C. Archer, V. Cameron, M. B. Andersen, M. J. Rijkenberg, and T. W. Lyons. 2016. The oceanic budgets of nickel and zinc isotopes: The importance of sulfidic environments as illustrated by the Black Sea. Philos. Trans. A Math. Phys. Eng. Sci. **374**: 20150294. doi:10.1098/rsta.2015.0294

Viollier, E., D. Jézéquel, G. Michard, M. Pèpe, G. Sarazin, and P. Alberic. 1995. Geochernical study of a crater lake (Pavin Lake, France): Trace-element behaviour in the monimolimnion. Chem. Geol. **125**: 61–72. doi:10.1016/0009-2541(95)00059-U

Viollier, E., G. Michard, D. Jézéquel, M. Pèpe, and G. Sarazin. 1997. Geochemical study of a crater lake: Lake Pavin, Puy de Dôme, France. Constraints afforded by the particulate matter distribution in the element cycling within the lake. Chem. Geol. **142**: 225–241. doi:10.1016/S0009-2541(97)00093-4

Vogel, H., J. M. Russell, S. Y. Cahyarini, S. Bijaksana, N. Wattrus, J. Rethemeyer, and M. Melles. 2015. Depositional modes and lake-level variability at Lake Towuti, Indonesia, during the past∼ 29 kyr BP. J. Paleolimnol. **54**: 359–377. doi:10.1007/s10933-015-9857-z

von Rintelen, T., K. von Rintelen, M. Glaubrecht, C. D. Schubart, and F. Herder. 2012. Aquatic biodiversity hotspots in Wallacea: The species flocks in the ancient lakes of Sulawesi, Indonesia, p. 290–315. *In* D. Gower, K. Johnson, J. Richardson, B. Rosen, L. Rüber, and S. Williams [eds.], Biotic evolution and environmental change in Southeast Asia, 1st ed. Cambridge Univ. Press. doi:10.1017/CBO9780511735882.014

Vuillemin, A., M. A. Morlock, A. Paskin, L. G. Benning, C. Henny, J. Kallmeyer, J. M. Russell, and H. Vogel. 2023. Authigenic minerals reflect microbial control on pore waters in a ferruginous analogue. Geochem. Perspect. Lett. **28**: 20–26. doi:10.7185/geochemlet.2339

Waite, T. D., J. A. Davis, T. E. Payne, G. A. Waychunas, and N. Xu. 1994. Uranium (VI) adsorption to ferrihydrite: Application of a surface complexation model. Geochim. Cosmochim. Acta **58**: 5465–5478. doi:10.1016/0016-7037(94)90243-7

Wei, W., R. Klaebe, H. F. Ling, F. Huang, and R. Frei. 2020. Biogeochemical cycle of chromium isotopes at the modern Earth's surface and its applications as a paleo-environment proxy. Chem. Geol. **541**: 119570. doi:10.1016/j.chemgeo.2020.119570

Wen, H., J. Carignan, X. Chu, H. Fan, C. Cloquet, J. Huang, Y. Zhang, and H. Chang. 2014. Selenium isotopes trace anoxic and ferruginous seawater conditions in the Early Cambrian. Chem. Geol. **390**: 164–172. doi:10.1016/j.chemgeo.2014.10.022

Wilson, M. E., and S. J. Moss. 1999. Cenozoic palaeogeographic evolution of Sulawesi and Borneo. Palaeogeogr. Palaeoclimatol. Palaeoecol. **145**: 303–337. doi:10.1016/S0031-0182(98)00127-8

Wüest, A., G. Piepke, and J. D. Halfman. 1996. Combined effects of dissolved solids and temperature on the density stratification of Lake Malawi, p. 183–202. *In* Limnology, climatology and paleoclimatology of the East African lakes. Routledge.

Xiong, Y. 2003. Solubility and speciation of rhenium in anoxic environments at ambient temperature and applications to the Black Sea. Deep-Sea Res. I. Oceanogr. Res. Pap. **50**: 681–690. doi:10.1016/S0967-0637(03)00037-2

Yeghicheyan, D., and others. 2019. A new interlaboratory characterisation of silicon, rare earth elements and twenty-two other trace element concentrations in the natural river water certified reference material SLRS-6 (NRC-CNRC). Geostand. Geoanal. Res. **43**: 475–496. doi:10.1111/ggr.12268

Zegeye, A., and others. 2012. Green rust formation controls nutrient availability in a ferruginous water column. Geology **40**: 599–602. doi:10.1130/G32959.1

Acknowledgments

This project was made possible by the invaluable support of Herson Rare's and many local residents living at Lake Poso who enabled the fieldwork, and we are grateful for their assistance. We thank Patrick Kathriner, Mike Chan, and Marcel Walter for assistance in sample analysis, and Tomy Doda and Damien Bouffard for assistance with calculations of density and physical interpretations. We also thank Tomy Doda for helpful discussions and quantification of stratification metrics. We thank Beat Müller for helpful discussions of the geochemical modeling. This manuscript was improved through constructive comments from Editor-in-Chief K. David Hambright; Associate Editor Werner Eckert, and three anonymous reviewers, and we thank them for their insight and helpful critiques. This project was carried out with support from the Swiss National Science Foundation through research grant 200021_153053 to HV as well as 200021_219223 to DJJ. We thank the National Research and Innovation Agency (BRIN) of Indonesia for facilitating this project through foreign

19395590, 2024, 11, Downloaded from https://aslopubs.onlinelibrary.wiley.com/doi/10.1002/lno.12687 by Paul Scherrer Institut PSI, Wiley Online Library on [02/12/2024]. See the Terms and Conditions (https://onlinelibrary.wiley.com/terms-and-conditions) on Wiley Online Library for rules of use; OA articles are governed by the applicable Creative Commons License

research permit 43A/SIP/IV/FR/9/2022. Open access funding provided by ETH-Bereich Forschungsanstalten.

Conflict of Interest

The authors declare that they have no known conflicts of interest that could appear to influence this manuscript.

Submitted 12 August 2024
Revised 25 August 2024
Accepted 30 August 2024

Associate Editor: Werner Eckert

19395590, 2024, 11, Downloaded from https://aslopubs.onlinelibrary.wiley.com/doi/10.1002/lno.12687 by Paul Scherrer Institut PSI, Wiley Online Library on [02/12/2024]. See the Terms and Conditions (https://onlinelibrary.wiley.com/terms-and-conditions) on Wiley Online Library for rules of use; OA articles are governed by the applicable Creative Commons License